White Paper

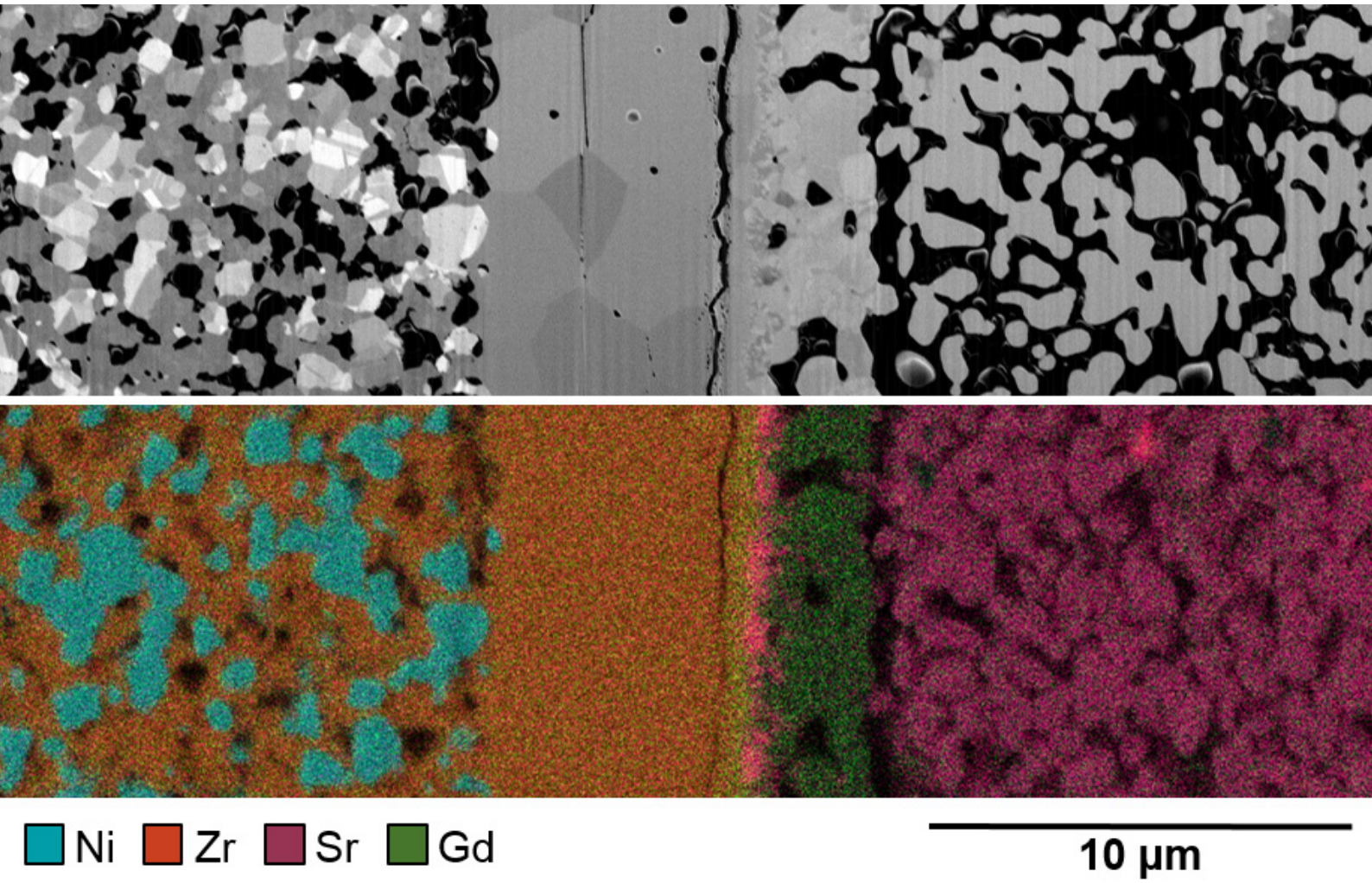

Characterization of Solid Oxide Electrolysis Cells by Advanced FIB-SEM Tomography

ZEISS Atlas 5

Characterization of Solid Oxide Electrolysis Cells by Advanced FIB-SEM Tomography

ZEISS Atlas 5

Authors: Marco Cantoni
Centre Interdisciplinaire de Microscopie Électronique, École Polytechnique Fédérale de Lausanne (EPFL)

Arata Nakajo, Giorgio Rinaldi, Stefan Diethelm, Jan van Herle
Institute of Mechanical Engineering, SCI-STI-JVh Group of Energy Materials (GEM), École Polytechnique Fédérale de Lausanne (EPFL)

Fabián Pérez-Willard
Carl Zeiss Microscopy GmbH

Date: June 2017

Microstructural changes after cycling of a solid oxide electrolysis cell (SOEC) were studied by means of FIB-SEM tomography. The advanced tomography package ZEISS Atlas 5 3D Tomography allows high resolution 3D electron imaging and 3D EDS elemental imaging using two different sets of SEM conditions optimized for the respective task. The additional chemical information facilitated the correct segmentation of the different phases present in the sample. This was crucial to better understand the diverse mechanisms leading to deterioration of the cell.

Introduction

Solid oxide electrolysis cells (SOEC) constitute a promising alternative to batteries for the storage of excess renewable energy, reaching close to 100% electrical-to-H_2 efficiency. In the SOEC, gaseous water is split into pure oxygen and hydrogen by high-temperature electrolysis [1]. The hydrogen can then be stored and used as an environmentally clean zero-emission fuel.

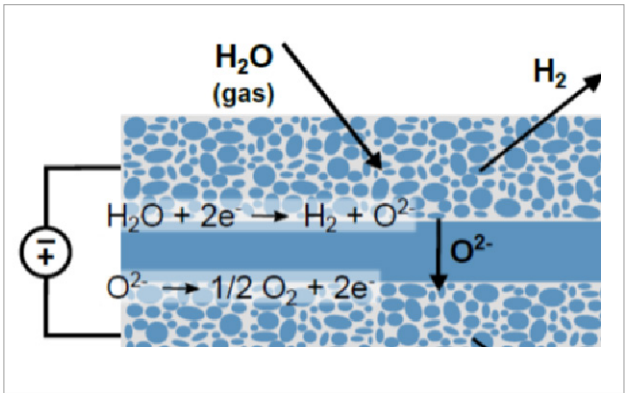

Figure 1: *Schematic showing the principle of operation of a SOEC.*

The SOEC is built up from different ceramic layers (Figure 1). The electrolyte between cathode and anode is dense and only a few micrometers thick, while the electrodes are thicker and porous to allow gas transport. Steam is fed to the SOEC at the cathode side. By the application of a sufficient voltage difference between the electrodes, the steam is reduced at the cathode-electrolyte interface yielding hydrogen gas and oxygen ions. The oxygen ions travel through the dense electrolyte to the anode where they are released after oxidation as oxygen gas.

SOECs are operated at temperatures between 500°C and 800°C. At such temperatures, chemical interdiffusion at interfaces and morphological or crystallographic changes can happen, which leads to a degradation of the cell performance over time. An important goal of current research on SOECs is to extend their lifetimes. Today, performance loss rates are in the region of a few percent per year. However, this is not good enough for a broad adoption of this new technology and further improvements are necessary.

In this context, three-dimensional (3D) X-ray- and focused ion beam scanning electron microscopy (FIB-SEM) [2, 3] play a key role

as they enable researchers to track changes in the device morphology and topology caused by its operation, such as microstructural coarsening or the formation of undesired phases, across different relevant length scales. In this study, we combine FIB-SEM tomography with chemical energy dispersive spectroscopy (EDS) to study the ageing of a SOEC.

Sample

The cell imaged by FIB-SEM/EDS comprises an yttria-stabilized zirconia (YSZ) electrolyte, a heterogeneous Ni-YSZ hydrogen electrode, a single solid phase lanthanum strontium cobalt (LSC) oxygen electrode and a gadolinia-doped ceria (GDC) compatibility layer to prevent reaction between the YSZ electrolyte and the LSC electrode.

The sample was extracted from a 6-cell stack operated during 11'300 h in steam electrolysis at 710°C and 0.5 – 0.6 A cm^{-2} [4]. The degradation was severe during the initial 2'000 h, with a voltage increase rate of 4%/kh on average and then stabilized at <0.5%/kh. The stack survived accidental water interruption incidents and was stopped after the 4^{th} one.

A cell sample was extracted from the stack and fractured to expose the interfaces between the electrodes and the electrolyte. The sample was impregnated with EPON812, polished first mechanically, and then by ion-milling.

FIB-SEM Tomography with Atlas 5

During FIB-SEM tomography, the FIB is used to produce cross sections perpendicular to the surface of the sample (Figure 2a). The sample is located at the intersection point of FIB and SEM beams (at an angle of 54° with respect to each other), and therefore, the cross sections can be imaged by SEM immediately after or during cutting without moving the sample [5]. The process of removing a thin slice of material by FIB and imaging the freshly exposed cross section by SEM is usually iterated many times: A stack of image results, where each image corresponds to one section, or slice, of the volume of interest (VOI). A 3D model of the VOI can be reconstructed digitally from the image data.

The 3D resolution of the FIB-SEM tomogram is determined by the resolution of the SEM images (XY plane), and in Z direction by the SEM excitation depth and the slice thickness control. It is a great experimental challenge to obtain a resolution in Z that matches the XY SEM resolution of typically just a few nanometers. This raises two fundamental questions: First, what is the minimal slice thickness that one can reasonably probe with the SEM?

In order to avoid signal convolution across slices, the information depth needs to be of the order of the targeted slice thickness, or ideally smaller (Figure 2b). Energy selective backscattered (EsB) electron imaging at low voltage (< 2 kV) is the most surface-sensitive imaging technique in SEM. The Inlens EsB detector features a high pass energy filter, which is open only for electrons within a small energy window below the primary landing energy (low-loss electrons). These originate from very surface near regions. Monte Carlo simulations prove that EsB signals probe less than 3 nm deep into silicon for 1 keV landing energy and an energy window of 100 eV [6].

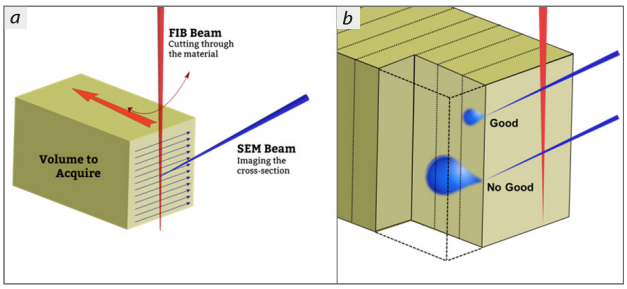

Figure 2: *(a) Schematic of a sample during FIB-SEM tomography. (b) Illustration showing the VOI and volume probed by the SEM. The dotted lines correspond to the location of the different sections of the tomogram.*

Conversely, 3D EDS spatial resolution is much lower. For a given SEM landing energy, the interaction volume for X-ray generation is inherently larger than that for secondary or backscattered electron generation. Further, while FIB-SEM tomography provides its best spatial resolution when performed at low accelerating voltages, EDS requires larger landing energies for the excitation of the characteristic EDS fingerprint. Therefore, depending on the sample, elements of interest, and slice thickness, typically it is enough to acquire EDS data only every 5 to 20 tomogram slices.

The advanced FIB-SEM tomography solution Atlas 5 used for this experiment can switch automatically between two different sets of SEM conditions: a first set, at low voltage and current, for the acquisition of high-resolution electron images with smallest possible voxel sizes, and a second set, at much higher voltage and current, for high-throughput

EDS mapping with lower spatial resolution [7]. Thus, 3D electron imaging resolution is not sacrificed by the EDS analysis.

The second question is: is it possible to control material removal by FIB to reproducibly cut slices just a few nanometer thick from the VOI? For this purpose, Atlas 5 uses fiducial marks patterned by FIB on the sample surface above the VOI (Figure 3). Atlas 5 uses the central trio of lines to perform drift correction, auto-focus and auto-stigmation functions during the experiment. The two outermost lines are used to measure the slice thickness by simply tracking their distance change between consecutive cross sections. Atlas 5 will adapt the speed of material removal according to the measured slice thickness during the run to ensure homogeneously spaced sections. Isometric voxels of down to 3 nm have been reported using Atlas [8].

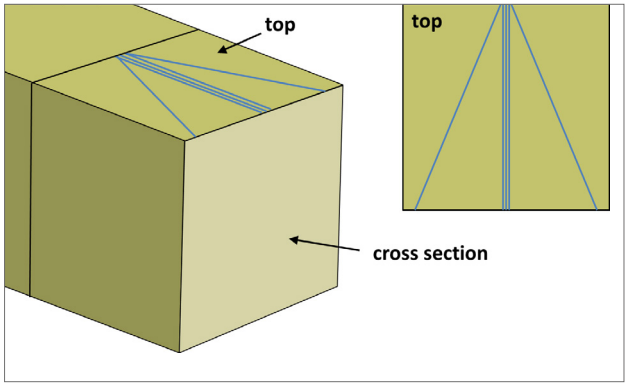

Figure 3: *Perspective and top view of the VOI. The outer blue lines are fiducials used for adaptive tracking of the slice thickness. The central lines are used for drift correction, auto-focus and auto-stigmation.*

Experiment

FIB-SEM tomography data from the secondary electron / secondary ion detector (SESI) and the Inlens EsB detector was recorded at an acceleration voltage of 1.8 kV on the SOEC sample. Before the acquisition, fiducial marks were milled to adjust the position of the FIB beam and guarantee isometric voxels of 10 nm, with a precision in the range of 1 nm. In addition, every 10 slices, the acceleration voltage was automatically switched from 1.8 kV to 10 kV for the acquisition of EDS elemental maps. The EDS voxel size was chosen to be 40 × 40 × 100 nm^3 to match in a first order approximation the larger interaction volume when in EDS conditions. The voltage of 10 kV allows detection of all relevant elements present in the sample, namely Ni, Y, Zr, O, La, Sr, Gd, and Ce. The reconstructed volume was 38 × 10 × 11 μm^3.

As an example, Figure 4 shows a SESI image and the corresponding EDS dataset. A total of 1100 sections were prepared and 110 EDS maps collected. Each section of the tomogram was imaged acquiring SESI and EsB signals in parallel.

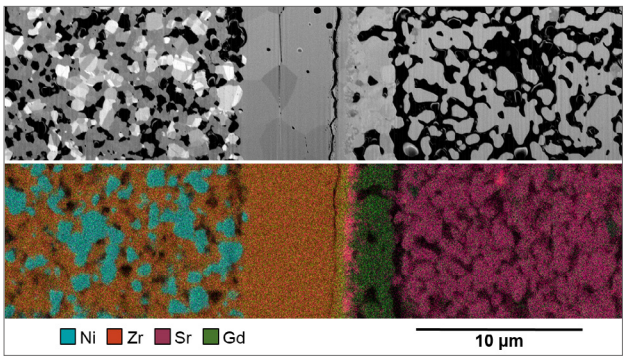

Figure 4: *SESI (top) and EDS (bottom) images of an exemplary slice of the SOEC tomography dataset.*

The three central notches used for drift correction, auto-focus and auto-stigmation during the tomography run (see Figure 3) were also used for post-acquisition fine alignment of the electron images with respect to each other. The EDS maps were then registered with the aligned SEM dataset and resampled at a voxel size of 10 nm. The segmentation of the data, which consists in assigning to each voxel belonging to a same material phase the same label, was performed using Matlab routines with calls to a software for data visualization and analysis (Avizo) for image gradient and watershed transform computations. The markers for each of the pore, Ni, YSZ, Ce and Sr-containing phases were generated by combining the SESI and EDS dataset.

Figure 5 shows a 3D view of the labelled imaged (color-coded) volume with improvement of the markers for the watershed-based segmentation with the EDS information.

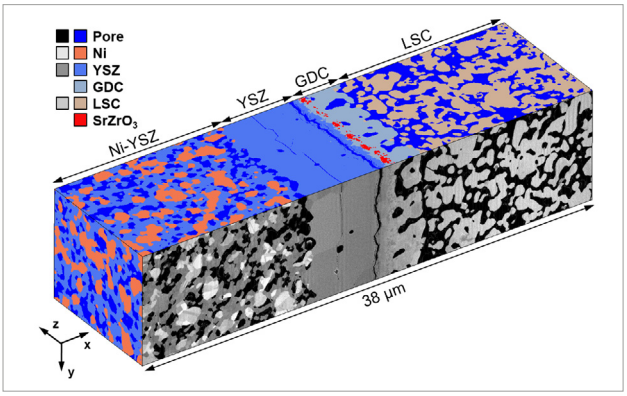

Figure 5: *3D reconstruction of the VOI.*

Discussion

SOEC post-test analyses show enhanced Zr and/or Sr cation diffusion across the electrolyte layers, delamination and Ni redistribution close to the electrolyte, resulting in a higher degradation rate, compared with solid oxide fuel cell (SOFC) conditions. The current understanding partly explains the difference in behavior qualitatively, but the exact nature of the phenomena and the driving forces remain imprecisely known [9, 10]. 3D imaging at high spatial resolution with advanced capabilities for elemental mapping is therefore key to understanding the multiple transport phenomena that occur across the layers under gradients of electrochemical potential in operation.

3D elemental information first allows the improvement of the segmentation. Ni grains that cannot be distinguished from the YSZ phase in the SESI data because of orientation or percolation can be segmented accurately (Figure 4). The EDS data also allows the distinction of the GDC, LSC and YSZ phases (Figure 5).

Significant microstructural degradation was observed in the 11'000 h SOEC sample. The GDC interlayer partially prevents the formation of a layer of $SrZrO_3$ insulating secondary phase, which grows faster than in SOFC operation and increases the ohmic losses within the cell. The difference is potentially due to the difference in the vacancy concentration within the oxygen electrode in SOFC and SOEC mode and/or Zr diffusion resulting in closed porosities forming along the grain boundaries in the YSZ electrolyte. The formed secondary phases and closed porosity both affect the resistance of the cell against thermal cycling. In the present sample, the weakening of the interface resulted in delamination over a large area that impedes the transport of oxygen ions. Even though cracking might have occurred during sample preparation or the uncontrolled water interruption events, similar failures are typically not seen in pristine and SOFC samples. The observations indicate that the development of cost-effective methods for the deposition of dense interlayers and likely the control of the oxygen vacancy concentration in the oxygen electrode by manipulation of the SOEC stack operating conditions are key to extend the lifetime of SOEC devices.

Micro-cracking is also observed in the LSC electrode and inter-phase cracks in the Ni-YSZ electrode, predominantly close to the YSZ electrolyte. The contiguity of the phases is not significantly affected, but the cracks might still alter the transport pathways to the electrocatalytic sites locally within the electrochemically-active regions. The transport properties of the Ni phase and the density of triple-phase boundary sites in the Ni-YSZ are affected by microstructural coarsening. In the present sample, the depletion of Ni is observed close to the YSZ interface. At present, the exact reasons for micro-cracking and Ni depletion remain unknown.

Conclusion

Advanced FIB-SEM tomography was used to reveal structural changes in an aged SOEC. The chemical EDS information included in the 3D dataset allowed the different phases present in the sample to be correctly segmented. This was crucial to achieve a better understanding of the mechanisms leading to cell deterioration.

The 3D FIB-SEM/EDS capability presented enables the measurement of metric and topological properties and directs discrete-element simulations, to first quantify the extent of microstructural changes and second accurately quantify the detrimental effect on the cell performance.

These analyses will be performed in the near future on the segmented data to improve the knowledge on SOEC degradation and provide precise guidance for both microstructural design and stack operation strategies.

References:

1. A. Vojvodic and J. K. Nørskov, Optimizing Perovskites for the Water-Splitting Reaction, Science 334 (2011), pp. 1355-1356.
2. J.R. Wilson et al., Three-Dimensional Reconstruction of a Solid Oxide Fuel Cell Anode, Nat. Mater. 5 (2006), pp. 541–544.
3. G.J. Nelson et al., Comparison of SOFC cathode microstructure quantified using X-ray nanotomography and focused ion beam-scanning electron microscopy, Electrochem. Commun., 13 (2011), pp. 586-589.
4. G. Rinaldi et al., Post-test Analysis on a Solid Oxide Cell Stack Operated for 10,700 Hours in Steam Electrolysis Mode, Fuel Cells (2017) in press.
5. M. Cantoni and L. Holzer, Advances in 3D focused ion beam tomography, MRS Bulletin 39 (2014), pp. 354-360.
6. Not shown. Results obtained using the Monte Carlo simulation software CASINO. See: D. Drouin et al., Scanning 29 (2007), pp. 92-101.
7. K. Narayan et al., Multi-resolution correlative focused ion beam scanning electron microscopy: applications to cell biology, J. Struct. Biol. 185 (2014), pp. 278-284.
8. M. Cantoni et al., Proceedings of the 16th European Microscopy Congress, Lyon, France (2016).
9. F. Tietz et al., Degradation phenomena in a solid oxide electrolysis cell after 9000 h of operation, J. Power Sources 223 (2013), pp. 129-135.
10. D. The et al., Microstructural comparison of solid oxide electrolyser cells operated for 6100 h and 9000 h, J. Power Sources 275 (2015), pp. 901-911.

Carl Zeiss Microscopy GmbH
07745 Jena, Germany
microscopy@zeiss.com
www.zeiss.com/microscopy